Electronic Supplementary Material (ESI) for Dalton Transactions.
This journal is © The Royal Society of Chemistry 2019

Temperature-assisted formation of reversible metallophilic Au-Ag interaction arrays

María Gil-Moles,[a] M. Concepcion Gimeno,*[b] José M. López-de-Luzuriaga,*[a] Miguel Monge,[a] and M. Elena Olmos,[a]

Electronic Supplementary Information

a Departamento de Química, Universidad de La Rioja, Centro de Investigación de Síntesis Química (CISQ), Complejo Científico Tecnológico, 26004 Logroño, Spain.
b Departamento de Química Inorgánica, Instituto de Síntesis Química y Catálisis Homogénea (ISQCH), CSIC-Universidad de Zaragoza, E-50009 Zaragoza, Spain.

Table of contents

I. Experimental section S2

1. General S2
2. Instrumentation S2
3. Synthesis S2

II. Optical properties S3

1. UV-Vis absorption spectra in solution (Figure S1) S3
2. Luminescence in solid state (Figure S2) S3

III. Experimental details S4

1. PSGE measurements (Figure S3) S4
2. Conductivity measurements (Tables S1 and S2) S6

IV. Crystallography S8

1. Single crystal X-ray **2b** (Tables S3-S6 and Figures S4-S6) S8
2. Powder X-ray diffraction analysis of compound **2a** (Figure S7) S13

V. References S13

I. Experimental section

1. General: ,2´:6´2´´–terpyridine and $AgOSO_2CF_3$ were purchased from Alfa Aesar and used as received. $NBu_4[Au_2(C_6F_5)_2]$ were prepared according to the literature.[1S]

2. Instrumentation: Fourier transform infrared (FT–IR) spectra were recorded in the 4000–450 cm^{-1} range on a PerkinElmer μ–ATR Spectrum II. C, H, and N analyses were carried out with PerkinElmer 240C microanalyzer. Molar conductivity measurements were carried out using a Crison Basic 30 conductimeter with a JULABO Immersion cooler system FT902 for controlling the temperature. Mass spectra were recorded on a HP–5989B API Electrospray mass spectrometer with 59987A interface; exact mass experiments were carried out in the same instrument as ESI mass experiments, and a Bruker Microflex matrix–assisted laser desorption ionization time–of–flight mass spectrometer (MALDI–TOF MS) using 11–dicyano–4–tert–butylphenyl–3–methylbutadiene (DCTB) as matrix. ^1H and ^{19}F NMR spectra were recorded with a Bruker Avance 400 or ARX 300 spectrometers in $[D_2]$–Methylene Chloride. ^1H PGSE measurements were carried out with the double stimulated echo pulse sequence (Double STE)[2S] on a Bruker AVANCE 400 equipped with a BBI H–BB Z–GRD probe at 298K–213K without spinning. Absorption spectra in solution were recorded on a Hewlett–Packard 8453 diode array UV–Vis spectrophotometer. Diffuse reflectance UV−vis spectra of pressed powder samples diluted with KBr were recorded on a Shimadzu (UV–3600 spectrophotometer with a Harrick Praying Mantis accessory) and recalculated following the Kubelka−Munk function.

3. Synthesis:

Synthesis of $[Ag_2(terpy)_2](CF_3SO_3)_2$ (**1**): see ref 3S.

Synthesis of $[\{Au(C_6F_5)_2\}Ag(terpy)]_n$ ((**2a**) (**2b**)):
Polymorph **2a:** see ref 3S.

Polymorph **2b:** A suspension of complex **2a** (0.0280 g) in CH_2Cl_2 (50 mL) was filtered and concentrated under vacuum and crystallize at 280K. After 24h $[\{Au(C_6F_5)_2\}Ag(terpy)]_n$ was obtained like yellow crystals. Yield: 42%. Single crystals were obtained by slow diffusion of diethylether into CH_2Cl_2 at 280K.

^1H NMR (300 MHz, $[D_8]$–THF, ppm) δ 8.28 (d, 2H, H_1, $^3J_{H1–H2}$=4.32), 8.20 (m, 3H,H_4 + H_6), 8.12 (m, 2H, H_5), 7.96 (ddd, 2H, H_3, $^3J_{H3–H2}$ ~$^3J_{H3–H4}$=7.60, $^4J_{H3–H1}$=1.68), 7.39 (ddd, 2H, H_2, $^3J_{H2–H3}$=7.5, $^3J_{H2–H1}$=5, $^4J_{H2–H4}$=1.1). ^{19}F NMR (282 MHz, $[D_8]$–THF, ppm) δ –115.00 (m, 2F, F_o), –163.12 (m, 2F, F_m) –164.67 (m, 1F, F_p) . ^1H NMR (300 MHz, $[D_2]$–CH_2Cl_2, ppm) δ 8.50 (d, 2H, H_1, $^3J_{H1–H2}$=4.42), 8.15 (dd, 1H,H_6, $^3J_{H6–H5}$=8.77, $^3J_{H6–H5´}$=8.79) 8.05–7.98 (m, 4H, H_5 + H_4), 7.94 (ddd, 2H, H_3, $^3J_{H3–H2}$ ~$^3J_{H3–H4}$=7.36, $^4J_{H3–H1}$=1.72), 7.42 (ddd, 2H, H_2, $^3J_{H2–H3}$=7.33, $^3J_{H2–H1}$=5.05, $^4J_{H2–H4}$=1.42). ^{19}F NMR (282 MHz, $[D_2]$–CH_2Cl_2, ppm) δ –114.86 (m, 2F, F_o), –159.94 (m, 2F, F_m) –163.05 (m, 1F, F_p). MS (ESI+) *m/z*: calculated for $[\{Au(C_6F_5)_2\}Ag_2(terpy)_2]^+$= 1210.9511; found 1210.9508. MS (ESI–) *m/z*: calculated for $[Au(C_6F_5)_2]^-$ = 530.9500; found 530.9506. MALDI–TOF(+) *m/z*: $[Ag(terpy)]^+$ = 339.835, MALDI–TOF(–) *m/z*: $[Au(C_6F_5)_2]^-$ = 530.826.

Analytical data (%): $C_{27}H_{11}Ag_1Au_1F_{10}N_3$ (872.21) requires 37.18, C; 1.27, H; 4.82, N. Found: 36.86, C; 1.34, H; 4.53, N. FTIR: ν(Au–(C_6F_5)) at 1502, 954, 781 cm^{-1}; ν(ring mode vibrations) 1452 cm^{-1}; ν(C=N) 1628–1568 cm^{-1}; ν(=C–H) vibration bending 1013–992 cm^{-1}.

II. Optical properties:

1. UV-Vis absorption spectra in solution:

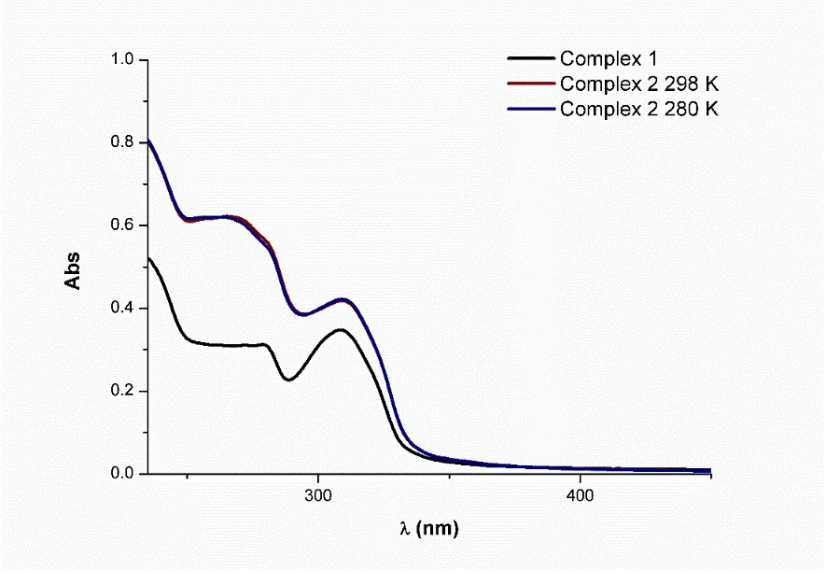

Figure S1: Absorption spectra in CH_2Cl_2 solutions of complexes **1** and **2** at 298K and 280K

2. Luminescence in solid state:

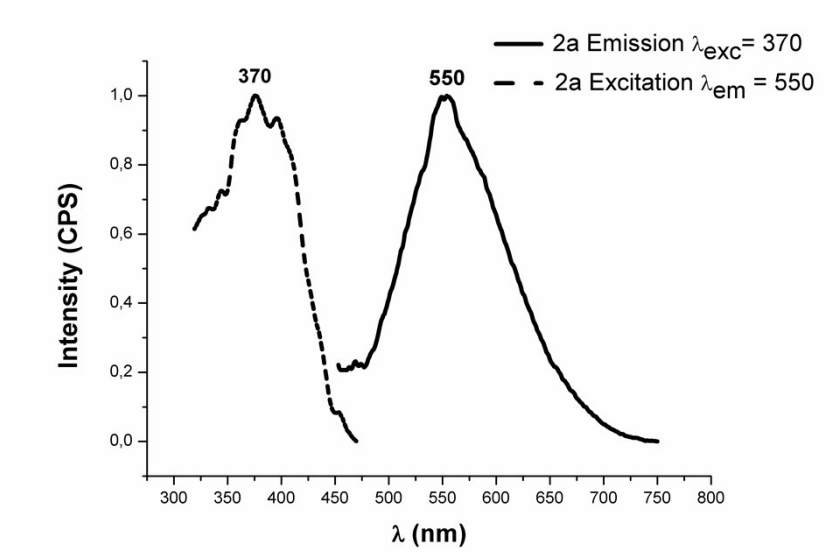

Figure S2: Luminescence in solid state at room temperature for complex **2a**.

III. Experimental details.

1. PGSE measurements:

^{1}H-PGSE measurements were carried out using the double stimulated echo pulse sequence (Double STE)[2S] on a Bruker AVANCE 400 equipped with a BBI H-BB Z-GRD probe at 298K–193K without spinning, using $[D_2]$ –CH_2Cl_2 as solvent.

When the double stimulated echo pulse sequence is used, the dependence of the resonance intensity *I* on a constant waiting time and on a varied gradient strength *G* is described by the equation (1):

$$I = I_0\, exp\left(- D_t (2\pi\gamma\delta G)^2 \left(\Delta - \frac{\delta}{3}\right) 10^4 \right) \quad (1)$$

Where *I* = intensity of the observed spin-echo, I_0 = intensity of the spin-echo without gradients, D_t = diffusion coefficient, Δ = delay between the midpoints of the gradients, δ = length of the gradient pulse, and γ = magnetogyric ratio.

The pulse sequence were composed of 90º pulses. The duration of the gradients (δ) was 2 ms, the delay Δ was 100 ms in cases 298K, 280K and Δ was 200 ms in the case of experiments at 253K, 233K and 213K, the strength *G* was varied during the experiment. The spectra were acquired using 40K points. The exponential plots of *I* versus *G* were fitted using a standard exponential regression algorithm implemented in TOPSPIN software.

PGSE data were treated[4S] using CH_2Cl_2 as internal standard, and introducing in the Stokes-Einstein equation (3) the semiempirical estimation of the *c* factor, which can be obtained through equation 2,[5S] derived from the microfriction theory proposed by Wirtz and co-workers,[6S] in which *c* is expressed as a function of the solute-to-solvent ratio of the radii.

$$c = \frac{6}{1 + 0.695\left(\frac{r_{solv}}{r_H}\right)^{2.234}} \quad (2)$$

$$D_t = \frac{kT}{c r_H \eta \pi} \quad (3)$$

Using the obtained diffusion coefficients D_t of the sample and the internal standard, and through the Stokes-Einstein equation (3), an accurate value of the hydrodynamic radius r_H can be obtained in each case[4S] and, once the hydrodynamic radius is known, the hydrodynamic volume V_H is calculated using equation (4).

$$V_H = \frac{4}{3}\pi r_H^3 \quad (4)$$

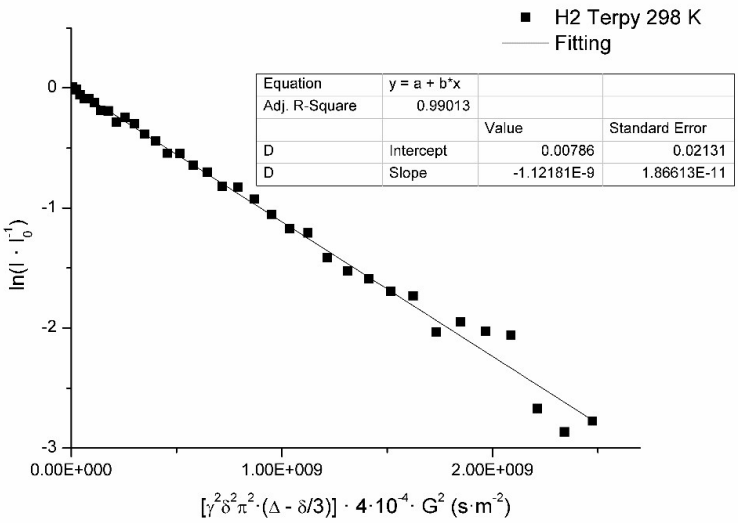
H2 Terpy 298 K
Fitting
Equation | y = a + b*x
Adj. R-Square | 0.99013
Value | Standard Error
D | Intercept | 0.00786 | 0.02131
D | Slope | -1.12181E-9 | 1.86613E-11
0
-1
-2
-3
ln(I · I0-1)
0.00E+000
1.00E+009
2.00E+009
[γ2δ2π2·(Δ - δ/3)] · 4·10-4· G2 (s·m-2)

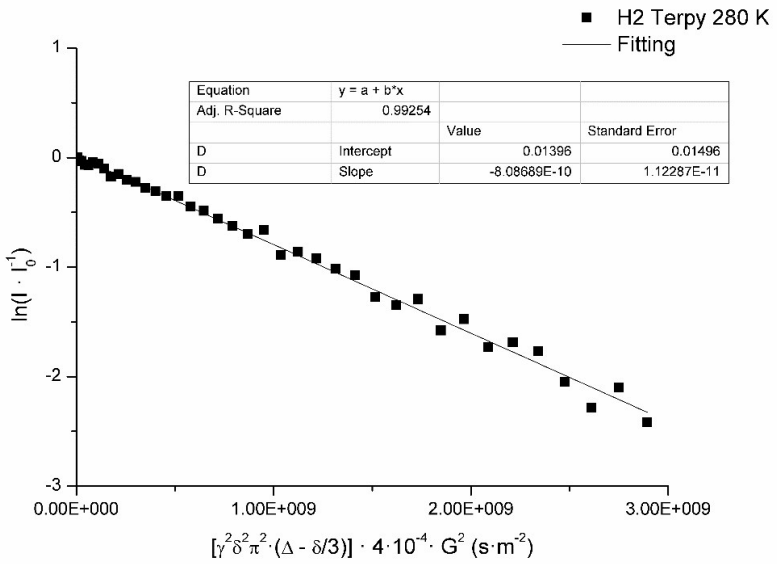
H2 Terpy 280 K
Fitting
Equation | y = a + b*x
Adj. R-Square | 0.99254
Value | Standard Error
D | Intercept | 0.01396 | 0.01496
D | Slope | -8.08689E-10 | 1.12287E-11
1
0
-1
-2
-3
ln(I · I0-1)
0.00E+000
1.00E+009
2.00E+009
3.00E+009
[γ2δ2π2·(Δ - δ/3)] · 4·10-4· G2 (s·m-2)

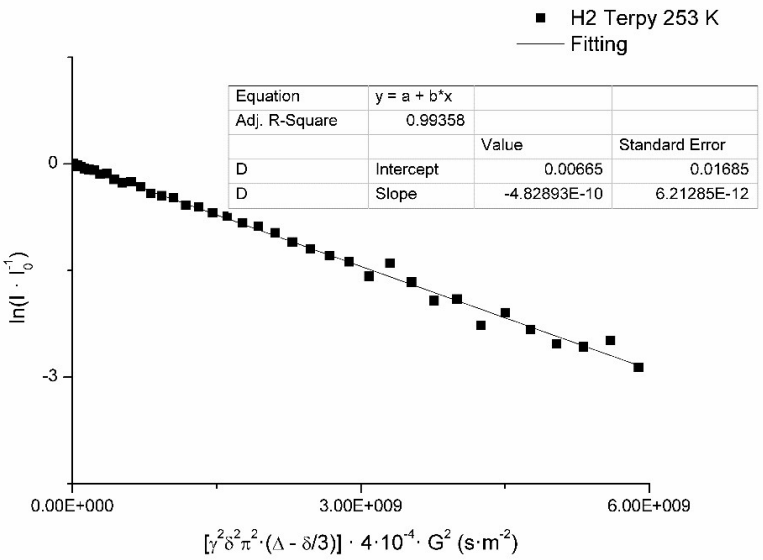
H2 Terpy 253 K
Fitting
Equation | y = a + b*x
Adj. R-Square | 0.99358
Value | Standard Error
D | Intercept | 0.00665 | 0.01685
D | Slope | -4.82893E-10 | 6.21285E-12
0
-3
ln(I · I0-1)
0.00E+000
3.00E+009
6.00E+009
[γ2δ2π2·(Δ - δ/3)] · 4·10-4· G2 (s·m-2)

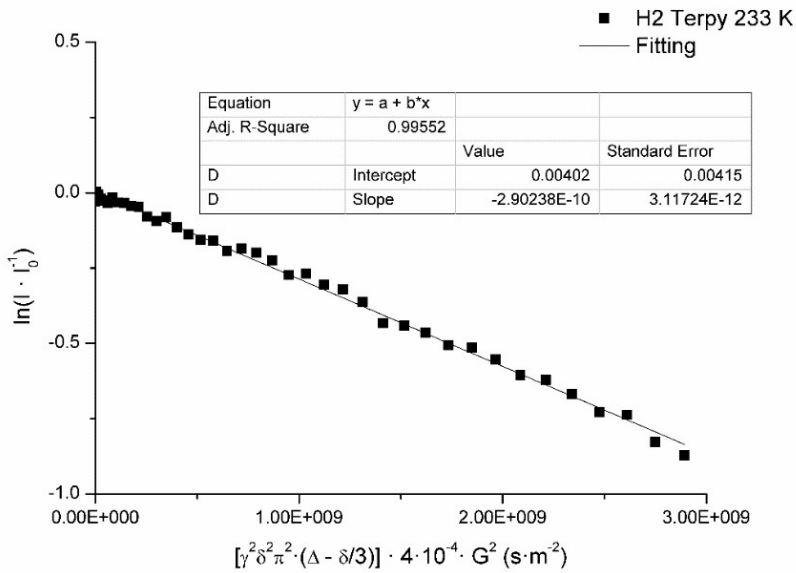

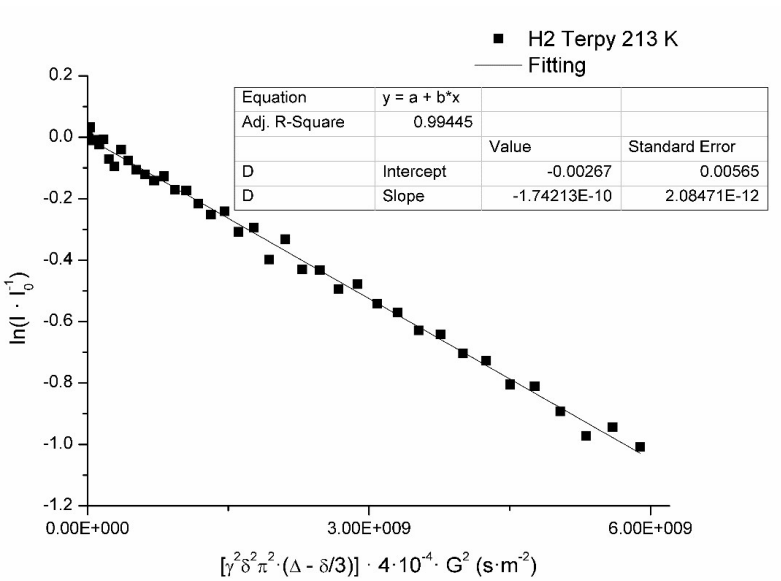

Figure S3: Graphics used to calculate D_t for complex **2**

2. Conductivity measurements:

Molar conductivity measurements were carried out using a Crison Basic 30 conductimeter of acetonitrile solutions of complex 2 in the 2 x 10^{-3} – 5 × 10^{-4} M range. All the measurements were carried out at 298K and at 293, 288, 283, 280, 273 and 263 K. In order to obtain comparable values, the results obtained at lower temperatures were compensated at 298 K with a compensation coefficient of 2%/ºC.

Using the Onsager law, $\Lambda_e = \Lambda_o - A\sqrt{c}$ (Λ_o molar conductivity at ∞ dilution, Λ_e molar conductivity, c concentration, and A is a coefficient that depends on the nature of the electrolyte, temperature and solvent) it is possible to estimate electrolyte type in solution. The Graphical representation Λ_e vs $\sqrt{c}$ gives the value of A (slope). Tabulated A values in acetonitrile provide the needed information (see ref 7S and Table S1). Table S2 shows the values of A obtained for complex 2 at different temperatures.

Table S1: Tabulated A values [7S] in CH_3CN at 298 K	
Electrolyte type	A
1:1	306-376
1:2	580-800
1:3	> 1200

Table S2: Values of the slopes A (linear fit following Onsager law model)

T (K)	Equation, r^2	A	Electrolyte
298	y = -773.9x +139.72 r^2 = 0.9782	773.9	1:2
293	y = -978.75x +149.01 r^2 = 0.9966	978.7	1:2-1:3
288	y = -1124x + 194.07 r^2 = 0.9641	1124	1:2-1:3
283	y = -1580.2x + 222.58 r^2 = 0.9827	1580	1:3
280	y = -1879,4x + 239,67 r^2 = 0,9712	1879	1:3
273	y = -2243.7x + 281.05 r^2 = 0.956	2243	1:3
263	y = -2927.8x + 405.99 r^2 = 0.9296	2927	1:3

IV. Crystallography:

1. Single crystal X-ray diffraction analysis of 2b.

The crystals were mounted in inert oil on a MiteGen MicroMount and transferred to the cold gas stream of a Nonius Kappa CCD (**2b·CH_2Cl_2**) or a Bruker APEX-II CCD (**2b·THF**) diffractometer equipped with an Oxford Instruments low–temperature attachment. Data were collected using monochromated MoKα radiation (λ = 0.71073 Å). Scan type: ω and ϕ. Absorption correction: semiempirical (based on multiple scans). The structure was solved by Direct Methods and refined on F^2 using the program SHELXL-97.[8S] All non–hydrogen atoms were refined anisotropically, with the exception of the disordered THF molecule in **2b·THF**. With the exception of the metal atoms, the whole molecule in **2b·THF**, as well as the dichloromethane molecule in **2b·CH_2Cl_2** are disordered over two different positions (50:50). Hydrogen atoms were included using a riding model. Further details of the data collection and refinement are given in Table S3 and selected bond distances and angles are shown in Tables S4 and S5. For more information, see: CCDC 1897914 and 1897915.

Table S3. Data collection and structure refinement details for **2b·CH_2Cl_2** and **2b·THF**

	2b·CH_2Cl_2	**2b·THF**
Chemical Formula	$C_{27}H_{11}AgAuF_{10}N_3 \cdot CH_2Cl_2$	$C_{27}H_{11}AgAuF_{10}N_3 \cdot OC_4H_8$
Crystal habit	Yellow needle	Yellow needle
Crystal size/mm	0.62 x 0.32 x 0.15	0.358 x 0.039 x 0.030
Crystal system	Triclinic	Triclinic
Space group	P-1	P-1
a/Å	10.8130(6)	10.8374(12)
b/Å	10.9768(4)	10.9982(10)
c/Å	12.9560(8)	14.0950(15)
α/°	80.139(3)	67.052(3)
β/°	86.040(2)	82.846(4)
γ/°	70.855(3)	71.245(3)
V/Å^3	1431.12(13)	1464.9(3)
Z	2	2
D_c/g cm^{-3}	2.221	2.141
M	957.15	944.33
F(000)	904	900
T/ºC	-100	-133
2θmax/°	55	56
μ(Mo-Kα)/mm^{-1}	6.082	5.766
No. refl. Measured	11028	23929
No. unique refl.	6407	5527
R_{int}	[R(int)=0.0830]	[R(int)=0.0398]
R[F>2σ(F)][a]	0.0366	0.0273
wR[F^2, all refl.][b]	0.0950	0.0543
No. of refl. Used [F>2σ(F)]	6407	5527
No. of parameters	424	666
No. of restrains	106	306
S [c]	1.023	1.029
Max. residual electron density/e·Å^{-3}	1.750	0.700

Table S4. Selected bond lengths (Å) and angles (°) for **2b·CH_2Cl_2**

Au(1)-Ag(1)	2.7969(3)	Ag(1)-N(1)	2.390(4)
Au(2)-Ag(1)	2.7747(3)	Ag(1)-N(2)	2.393(4)
Au(1)-C(16)	2.063(4)	Ag(1)-N(3)	2.427(4)
Au(2)-C(22)	2.045(5)	Ag(1)-C(16)	2.582(4)
C(16)-Au(1)-C(16)#1	180.0	N(1)-Ag(1)-C(16)	107.58(14)
C(22)-Au(2)-C(22)#2	180.0	N(2)-Ag(1)-C(16)	131.32(12)
Ag(1)-Au(1)-Ag(1)#1	180.0	N(3)-Ag(1)-C(16)	108.03(14)
Ag(1)-Au(2)-Ag(1)#2	180.0	N(1)-Ag(1)-Au(2)	92.85(9)
Au(2)-Ag(1)-Au(1)	160.167(16)	N(2)-Ag(1)-Au(2)	102.83(8)
C(16)-Au(1)-Ag(1)	62.02(11)	N(3)-Ag(1)-Au(2)	87.44(9)
C(16) -Au(1)-Ag(1)#1	117.98(11)	C(16)-Ag(1)-Au(2)	125.76(9)
C(22)-Au(2)-Ag(1)	92.93(12)	N(1)-Ag(1)-Au(1)	106.60(9)
C(22)-Au(2)-Ag(1)#2	87.07(12)	N(2)-Ag(1)-Au(1)	88.13(8)
N(1)-Ag(1)-N(2)	68.80(13)	N(3)-Ag(1)-Au(1)	81.43(9)
N(1)-Ag(1)-N(3)	135.48(14)	C(16)-Ag(1)-Au(1)	44.89(9)
N(2)-Ag(1)-N(3)	67.79(14)		

Symmetry transformations used to generate equivalent atoms: #1 -x+1,-y+1,-z #2 -x+1,-y+2,-z

Table S5. Selected bond lengths (Å) and angles (°) for **2b·THF**

Au(1)-Ag(1)	2.8090(4)	Ag(1)-N(2A)	2.484(4)
Au(2)-Ag(1)	2.7882(4)	Ag(1)-N(3)	2.395(2)
Au(1)-C(7A)	2.053(7)	Ag(1)-N(1B)	2.507(4)
Au(2)-C(1A)	2.071(4)	Ag(1)-N(2B)	2.482(4)
Au(1)-C(7B)	2.057(8)	Ag(1)-C(7A)	2.521(6)
Au(2)-C(1B)	2.073(4)	Ag(1)-C(7B)	2.520(5)
Ag(1)-N(1A)	2.512(4)		

C(7A)-Au(1)-C(7A)#1	180.0	N(2A)-Ag(1)-C(7A)	130.0(2)
C(1A)-Au(2)-C(1A)#2	180.0	N(3)-Ag(1)-C(7A)	107.6(2)
Ag(1)-Au(1)-Ag(1)#1	180.0	N(1B)-Ag(1)-C(7B)	109.6(2)
Ag(1)-Au(2)-Ag(1)#2	180.0	N(2B)-Ag(1)-C(7B)	130.1(2)
Au(2)-Ag(1)-Au(1)	158.513(14)	N(3)-Ag(1)-C(7B)	107.3(2)
C(7A)-Au(1)-Ag(1)	60.09(14)	N(1A)-Ag(1)-Au(2)	87.14(12)
C(7A)-Au(1)-Ag(1)#1	119.91(14)	N(2A)-Ag(1)-Au(2)	100.96(12)
C(7B)-Au(1)-Ag(1)	60.04(13)	N(3)-Ag(1)-Au(2)	93.47(8)
C(7B)-Au(1)-Ag(1)#1	119.96(13)	N(1B)-Ag(1)-Au(2)	87.09(12)
C(1A)-Au(2)-Ag(1)	86.07(18)	N(2B)-Ag(1)-Au(2)	100.94(12)
C(1A)-Au(2)-Ag(1)#2	93.93(18)	C(7A)-Ag(1)-Au(1)	44.90(15)
C(1B)-Au(2)-Ag(1)	93.98(17)	C(7B)-Ag(1)-Au(1)	45.01(17)
C(1B)-Au(2)-Ag(1)#2	86.02(17)	C(7A)-Ag(1)-Au(2)	128.86(17)
N(2A)-Ag(1)-N(1A)	64.51(15)	C(7B)-Ag(1)-Au(2)	128.85(19)
N(3)-Ag(1)-N(1A)	131.42(13)	N(1A)-Ag(1)-Au(1)	78.72(12)
N(3)-Ag(1)-N(2A)	67.75(12)	N(2A)-Ag(1)-Au(1)	87.56(11)
N(2B)-Ag(1)-N(1B)	64.69(16)	N(3)-Ag(1)-Au(1)	108.01(8)
N(3)-Ag(1)-N(1B)	131.51(13)	N(1B)-Ag(1)-Au(1)	78.79(12)
N(3)-Ag(1)-N(2B)	67.66(13)	N(2B)-Ag(1)-Au(1)	87.66(12)
N(1A)-Ag(1)-C(7A)	109.3(2)		

Symmetry transformations used to generate equivalent atoms: #1 -x+1,-y+1,-z #2 -x+1,-y,-z

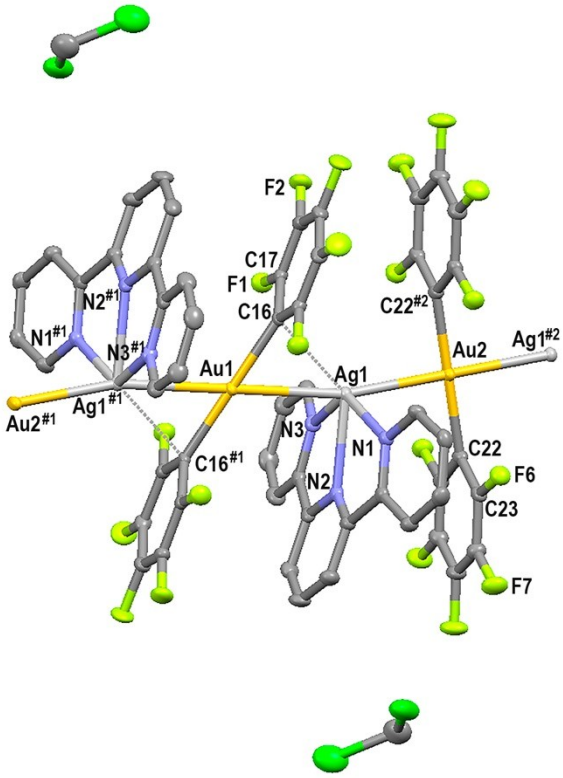

Figure S4: Part of the polymeric crystal structure of **2b·CH_2Cl_2**. Symmetry transformations used to generate equivalent atoms: #1 -x+1,-y+1,-z; #2 -x+1,-y+2,-z.

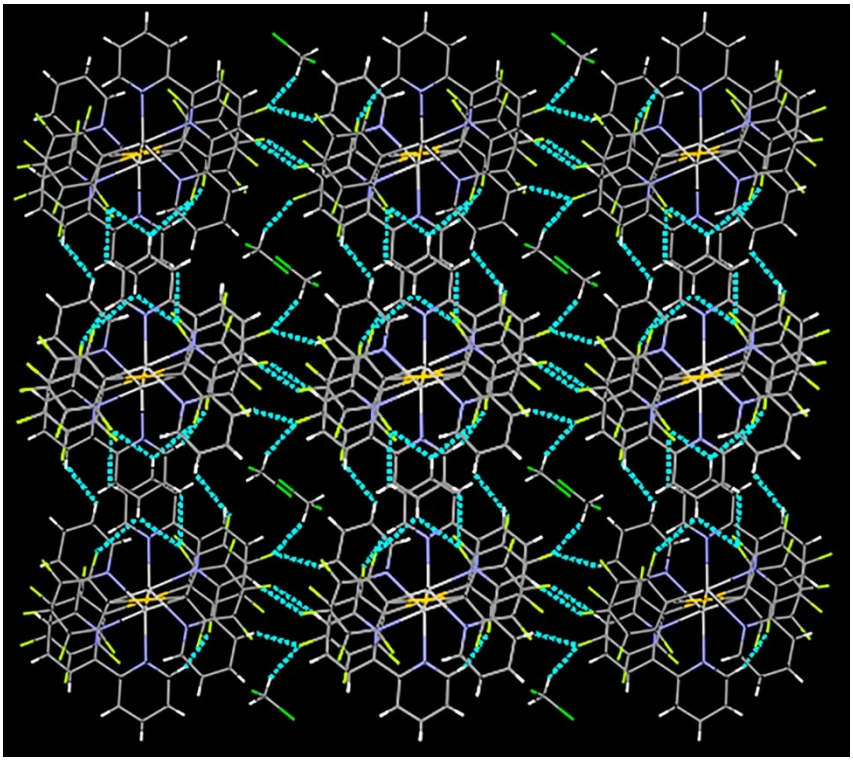

Figure S5: View of the 3D polymeric arrangement of **2b·CH_2Cl_2** through hydrogen bonds seen from the crystallographic *y* axis.

Table S6. Hydrogen bonds for **2b·CH$_2$Cl$_2$** (Å and °).

D-H...A	d(D-H)	d(H...A)	d(D...A)	<(DHA)
C(1)-H(1)...F(10)#2	0.93	2.54	3.309(6)	140.2
C(2)-H(2)...F(1)#3	0.93	2.60	3.189(6)	121.9
C(7)-H(7)...Cl(1B)#4	0.93	2.99	3.691(10)	133.6
C(9)-H(9)...F(3)#5	0.93	2.53	3.448(6)	168.0
C(12)-H(12)...F(8)#6	0.93	2.57	3.139(6)	120.0
C(14)-H(14)...F(7)#7	0.93	2.57	3.195(6)	124.6
C(28A)-H(28B)...F(8)#1	0.97	2.57	3.50(4)	160.8
C(3)-H(3)...F(1)#3	0.93	2.57	3.173(6)	122.7
C(12)-H(12)...F(3)#5	0.93	2.85	3.747(6)	162.6
C(15)-H(15)...F(6)#2	0.93	2.70	3.545(6)	152.0

Symmetry transformations used to generate equivalent atoms:

#1 -x+1,-y+1,-z; #2 -x+1,-y+2,-z; #3 x+1,y,z; #4 x+1,y,z-1; #5 x,y,z-1; #6 -x+1,-y+2,-z-1; #7 x-1,y,z

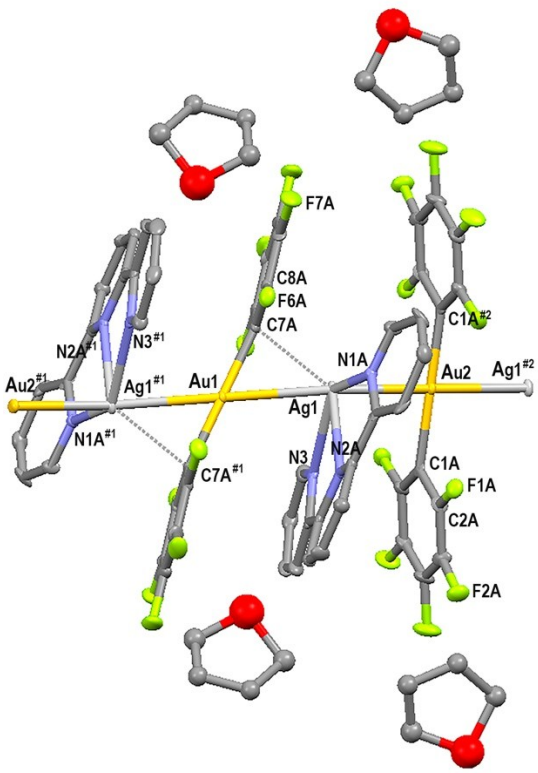

Figure S6: Part of the polymeric crystal structure of **2b·THF** with the labelling scheme for the atoms positions. Ellipsoids are drown at 30% level. Symmetry transformations used to generate equivalent atoms: #1 -x+1,-y+1,-z; #2 -x+1,-y,-z.

2. Powder X-ray diffraction analysis of compound 2a.

The Experimental X-ray powder pattern of complex **2a** obtained under synthesis conditions (solution in THF and precipitate with n-hexane) is matches with the theoretical X-ray powder patter of complex **2a** with crystals was obtained in CH_2Cl_2/Ether at 298 K see Figure S7.

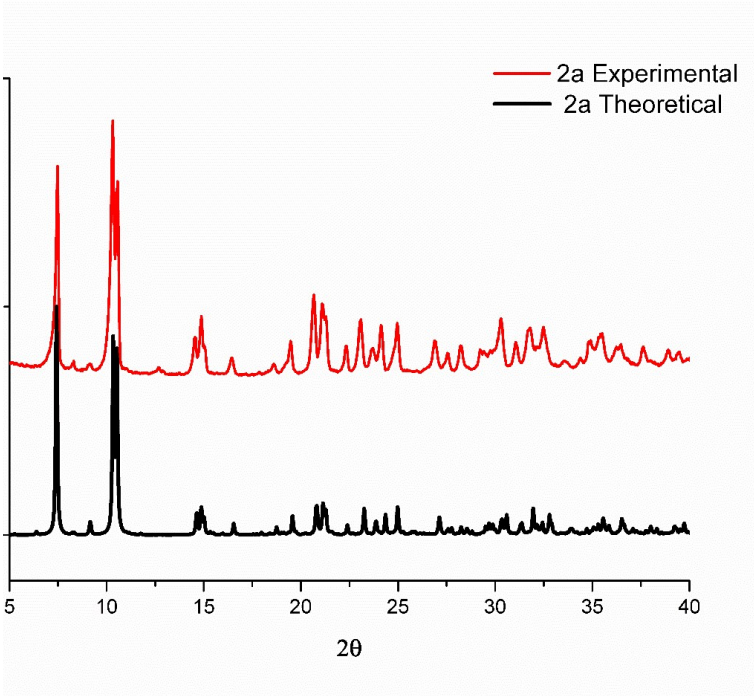

Figure S7: X-ray powder pattern for complex **2a**

V. References:

1S R. Usón, A. Laguna, J Vicente, *J. Organomet. Chem*. 1977, **131**, 471−475.

2S A. A. Khrapitchev, P. T. Callaghan, P. T., *J. Magn. Res*. 2001, **152**, 259–268

3S M. Gil-Moles, M. C. Gimeno, J. M. López-de-Luzuriaga, M. Monge, M. E. Olmos, D. Pascual, *Inorg. Chem*. 2017, **56**, 9281−9290.

4S a) D. Zuccaccia, A. Macchioni, *Organometallics*, 2005, **24**, 3476–3486. b) A. Macchioni,G. Ciancaleoni, C. Zuccaccia, D. Zuccaccia, *Chem. Soc. Rev*., 2008, **37**, 479–489.

5S a) H.-C. Chen, S.-H. Chen, *J. Phys. Chem.* 1984*,* **88**, 5118–5121; b) J. Espinosa, J. G. de la Torre, *J. Phys. Chem.* 1987*,* **91**, 3612–3616.

6S a) A. Gierer, K. Wirtz, *Z. Naturforsch*. A 1953, **8**, 522–532; b) A. Spernol, K. Wirtz, *Z. Naturforsch*. A 1953, **8**, 532–538.

7S L. Dutta, D. W. Meek, D. H. Busch, *Inorg. Chem*., 1970, **9**, 1215-1226.

8S G. M. Sheldrick, *SHELXL97, Program for Crystal Structure Refinement*, University of Göttingen, Germany, 1997.